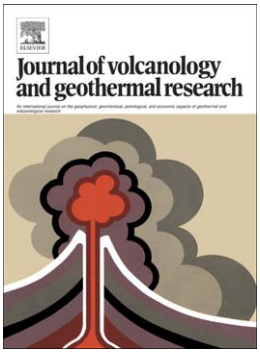

Forecasting volcanic ash dispersal and coeval resuspension during the April–May 2015 Calbuco eruption

F. Reckziegel, E. Bustos, L. Mingari, W. Báez, G. Villarosa, A. Folch, E. Collini, J. Viramonte, J. Romero, S. Osores

PII: S0377-0273(16)30076-2
DOI: doi: 10.1016/j.jvolgeores.2016.04.033
Reference: VOLGEO 5834

To appear in: *Journal of Volcanology and Geothermal Research*

Received date: 12 November 2015
Revised date: 13 April 2016
Accepted date: 29 April 2016

Please cite this article as: Reckziegel, F., Bustos, E., Mingari, L., Báez, W., Villarosa, G., Folch, A., Collini, E., Viramonte, J., Romero, J., Osores, S., Forecasting volcanic ash dispersal and coeval resuspension during the April–May 2015 Calbuco eruption, *Journal of Volcanology and Geothermal Research* (2016), doi: 10.1016/j.jvolgeores.2016.04.033

Forecasting volcanic ash dispersal and coeval resuspension during the April-May 2015 Calbuco eruption

F. Reckziegel [(1)], E. Bustos [(1)], L. Mingari [(2,3)], W. Báez [(1)], G. Villarosa [(4)], A. Folch [(5)], E. Collini [(3,6)], J. Viramonte [(1)], J. Romero [(7,8)], S. Osores [(2,3,9)]

(1) INENCO/GEONORTE, Univ. Nacional de Salta, CONICET, Salta, Argentina.

(2) Consejo Nacional de Investigaciones Científicas y Técnicas (CONICET), Buenos Aires, Argentina.

(3) Servicio Meteorológico Nacional (SMN), Argentina.

(4) INIBIOMA, CRUB (CONICET-Universidad Nacional del Comahue), Bariloche, Argentina.

(5) Barcelona Supercomputing Center (BSC), Barcelona, Spain.

(6) Servicio de Hidrografía Naval (SHN), Argentina.

(7) Departamento de Geología, Universidad de Atacama, Chile.

(8) Centro de Investigación y Difusión de Volcanes de Chile, Santiago, Chile.

(9) Comisión Nacional de Actividades Espaciales (CONAE), Buenos Aires, Argentina.

Abstract

Atmospheric dispersion of volcanic ash from explosive eruptions or from subsequent fallout deposit resuspension causes a range of impacts and disruptions on human activities and ecosystems. The April-May 2015 Calbuco eruption in Chile involved eruption and resuspension activities. We overview the chronology, effects, and products resulting from these events, in order to validate an operational forecast strategy for tephra dispersal. The modelling strategy builds on coupling the meteorological Weather Research and Forecasting (WRF/ARW) model with the FALL3D dispersal model for eruptive and resuspension processes. The eruption modelling considers two distinct particle granulometries, a preliminary first guess distribution used operationally when no field data was available yet, and a refined distribution based on field measurements. Volcanological inputs were inferred from eruption reports and results from an Argentina-Chilean ash sample data network, which performed in-situ sampling during the eruption. In order to validate the modelling strategy, results were compared with satellite retrievals and ground deposit measurements. Results indicate that the WRF-FALL3D modelling system can provide reasonable forecasts in both eruption and resuspension modes, particularly when the adjusted granulometry is considered. The study also highlights the importance of having dedicated datasets of active volcanoes furnishing first-guess model inputs during the early stages of an eruption.

Keywords: Volcanic ash, particle resuspension, dispersion model, Calbuco

1. Introduction

The April-May 2015 Calbuco eruption (Chile) affected vast regions of Argentina, with prevailing winds causing substantial tephra fallout in proximal locations and dispersal of ash clouds across the country. As occurred during the 2011 Cordón Caulle event (Folch et al., 2014), coeval resuspension of ash from fresh deposits highlighted the importance of this secondary hazard ~~in~~ at arid and windy areas such as the Argentinian Patagonia. Up to date, resuspension of ash from Calbuco deposits severely affects the normal development of activities on windy days, especially in the province of Neuquén (Argentina) and in the regions of Biobío, Araucanía, and Los Lagos (Chile). In Argentina, periodic episodes of resuspension are associated with the regional strong westerly winds. In Chile, episodes of resuspension are often related to the "Puelche", a warm easterly wind that blows across the Andes. These emissions of ash have caused periodic impacts on public health and agriculture and tourism sectors. The concentration of fine particles (PM_{10} and $PM_{2.5}$) frequently exceeds air quality standards (Folch et al., 2014) and environmental conditions during windy days often forced people to remain indoors. Schools in the region were closed for almost four months after the eruption.

Volcanic ash dispersal can trigger multiple impacts on human life and ecosystems (e.g. Wilson et al., 2011), including respiratory problems (Baxter, 1999), air quality deterioration, dysfunction of energy lines (Johnston et al., 2001), contamination of water bodies, or disruption of ground and air transportation networks. Volcanic ash poses a serious threat on civil aviation (e.g. Casadevall, 1993), compromising aircraft safety (Witham et al., 2007) and affecting the operability of airports (Guffanti et al., 2009). To face th~~i~~ese hazards, Volcanic Ash Advisory Centers (VAACs) make use of reports, observations and operational model forecasts to advise civil aviation authorities and stakeholders on the presence and evolution of ash clouds. In particular, the Buenos Aires VAAC uses the HYbrid Single-Particle Lagrangian Integrated Trajectory model (HYSPLIT, Draxler and Hess, 199~~7~~8) and the Eulerian FALL3D (Costa et al., 2006; Folch et al., 2009) models to forecast volcanic ash in the atmosphere under its area of responsibility (between 10°S-90°S latitude and 10°W-90°W longitude). Given the potential impact of ash resuspension in this region, a modelling strategy to forecast ash clouds from resuspension events is under development and evaluation for future transfer into operations.

This manuscript evaluates the operational modelling strategies for dispersion, deposition and resuspension of ash adopted during the April-May 2015 Calbuco eruption. To this purpose, simulations using the FALL3D model coupled off-line with the Weather Research Forecasting (WRF/ARW) Servicio de Hidrografía Naval - Servicio Meteorológico Nacional (SHN-SMN) model (experimental setup, Collini et al., 2013) are visually compared against Moderate Resolution Imaging Spectroradiometer (MODIS) imagery and ground deposit thickness observations. The

simulations resemble the syn-eruptive operational conditions, when few observations were available and most Eruption Source Parameters (ESPs) were uncertain during the first hours (or days) of the eruption. For this reason, our simulations build upon look-up tables of ESPs (e.g. Mastin et al., 2009) and preliminary data available at that time, including the granulometric distribution from the 1991 Hudson volcano eruption (Scasso et al., 1994) used by the Buenos Aires VAAC (GA, Osores et al., 2011). However, a second granulometry reconstructed from syn-eruptive field measurements~~,~~ is also considered in our simulations for comparison (GB).

In the following sections, this paper summarizes the geological background of the Calbuco volcano and gives a brief chronology of the April-May 2015 eruption, including the description of the resulting tephra fallout deposits. Secondly, we describe the modelling strategies for both eruption and resuspension ash cloud forecast. Simulation results are shown for two different model input granulometries (GA and GB) and compared against satellite and ground observations. Finally, conclusions are given highlighting the implications ~~on~~ for operational forecast~~s~~.

2. Geological b~~B~~ackground

Calbuco is a 2003 m a.s.l. height composite stratovolcano located on the Southern Andes of Chile (41°20'S, 72°37'W) (Fig. 1a). The Southern Volcanic Zone (SVZ; 37°-46°S) is characterized by a 30 km-thick continental crust, with dominant volcanic products basaltic and basaltic-andesitic in composition (Stern et al., 2004, and references therein). However, products from Calbuco volcano are mostly andesitic (Hickey-Vargas et al., 1995). The volcano morphology shows a truncated-cone shape and no significant major structures seem to control its activity.

The volcano basement comprises meta-sedimentary rocks (Upper Palaeozoic, Fig. 1b; Parada et al., 1987~~,~~; Thiele et al., 1985), plutonic rocks (tonalites, diorites and granites; Neogene; Parada et al., 1987; Munizaga et al., 1988) and Early Pleistocene volcanic and volcano-clastic sequences (Lahsen et al., 1985). The main edifice volume consists of blocky and "aa" type lava flows interbedded with pyroclastic rocks (López Escobar et al., 1992). Calbuco has suffered, at least, two sector collapses (towards the north and northwest) during the Holocene (Clavero et al., 2008). López Escobar et al. (1992) and Sellés and Moreno (2011) arranged the stratigraphy of the volcano taking into account its morphologic evolution in 4 units (named Calbuco 1, 2, 3 and 4; Fig. 1b) of mainly andesitic geochemical composition, recording its activity from Middle Pleistocene to present (Moreno, 1974; 1976; Lahsen et al., 1985; Hickey-Vargas et al., 1995; Sellés and Moreno, 2011). In this context, Calbuco 1 (Middle-Upper Pleistocene; ca. 340-110 ka) unit comprises porphyritic basaltic-andesite lava flows with volcanoclastic deposits interbedded emitted before the Würm glaciation. The main cone corresponds to andesitic lava flows belonging to Calbuco 2 (Upper Pleistocene, ca. 110-14.5

ka) unit. A violent eruption of this unit generated a debris-avalanche towards the NNW. Calbuco 2 unit enclosed three subunits: lava flows and pyroclastic rocks, flow and fall pyroclastic deposits and volcanic avalanche deposits. Calbuco 3 (Upper Pleistocene-Holocene, ca. <14 ka-1893 BC) is composed of lava flows interbedded with breccia and tuffs. Also, Alerce ignimbrite and volcanoclastic deposits are integrated in this unit. The stratigraphy of Calbuco 3 is completed by undifferentiated pyroclastic deposits and lahars and pre-historic pyroclastic flows. Finally, Calbuco 4 unit (Holocene) comprises the youngest history of the volcano, including the dome-cone and associated lava flows. Also, recent and historic lahars deposits are included. Also, during Holocene, moraines, fluvioglacial deposits, ancient fluvial deposits, recent fluvial deposits, marsh and lacustrine deposits, recent moraines, alluvial deposits, recent playa lake deposits and colluvial deposits are found.

3. Chronology and impacts of the April-May 2015 eruption

This section summarizes the chronology of the events occurred during the 2015 Calbuco eruption according to the Chilean OVDAS-SERNAGEOMIN daily reports. After decades of quiescence, a swarm of volcano-tectonic earthquakes started at Calbuco volcano on Wednesday 22 April at 15:11 LT (18:11 UTC). The hypocentres of this seismic activity were located beneath the eastern flank of the volcano, at about 7.4 km depth. Two hours later, long-period earthquakes related to fluid dynamics inside the volcano began to be recorded (SERNAGEOMIN, 2015a). At 18:04 LT (21:04 UTC) a first eruptive pulse lasting for ~90 minutes generated a greyish eruption column that during its paroxysmal phase rose up to 15 km above the crater (Fig. 2a) and drifted towards the north and northeast. After this first eruptive pulse, seismic signals returned to values close to the background noise until 21:55 LT (00:55 UTC), when seismic activity re-started moderately with a continuous harmonic tremor (SERNAGEOMIN, 2015b). On Thursday 23 April at 01:00 LT (04:00 UTC) a second eruptive pulse started accompanied by high-energy seismic signals formed by continuous harmonic tremors and volcano-tectonic earthquakes with an average of 150 events per hour. This second pulse occurred overnight, hindering the direct observation of the eruptive column but showing dramatic pulses of lightning. Despite this, a column height exceeding 15 km above the crater was reported by SERNAGEOMIN, with a direction of dispersion similar to the previous pulse (SERNAGEOMIN, 2015c). Preliminary estimates made by SERNAGEOMIN at 24 April based in the column height suggested that both pulses were sub-Plinian and ejected 0.04 km^3 and 0.17 km^3 of material respectively, but further estimates calculate a total erupted volume ranging from 0.28 to 0,58 km^3 (eg. Segura et al., 2015; Romero et al., 2016; Van Eaton et al., 2016). As a result of these pulses, approximately 6685 people were efficiently evacuated within a radius of 20 kilometres from the volcano summit and no fatalities occurred (SERNAGEOMIN, 2015c; Mella et

al., 2015). Partial eruption column collapses triggered pyroclastic density currents at the end of the first eruptive phase, but the largest occurred in the early hours of 23 April (Van Eaton et al., 2016) affecting the flanks of the volcano and headwaters of some rivers (Fig. 2b). Furthermore, the melting of the summit ice cap promoted the formation of primary lahars that affected the southern and north-northeastern flanks of the volcano (Blanco Sur, Blanco Este, Pescado y Tepu rivers) destroying some houses, bridges and salmon fisheries (Mella et al., 2015). The proximal lapilli-ash fallout blanket reached tens of centimetres at villages located north of the volcano (e.g. Ensenada), causing severe structural damages, roof collapses (Fig. 2c), and affecting livestock. After these two initial pulses, the volcano remained with moderated seismic activity and the plume of gas and ash did not exceed 1.5 km in height above the crater.

As a result of the ash clouds dispersion, many airports in Chile and Argentina were disrupted and a >14 of domestic and international flights were cancelled (Mella et al., 2015). In Chile, those regions north of the volcano (de Los Lagos, de Los Ríos and de La Araucanía) were the most affected by fallout, but ash at altitude was observed as far as in the metropolitan area of Santiago de Chile. In Argentina, the most affected localities were Junín de los Andes (Fig. 2d) and San Martín de Los Andes, while Villa La Angostura and Bariloche were less impacted than during the 2011 Cordón Caulle eruption. On Saturday 25 April the ash cloud reached Buenos Aires city and the south of Uruguay. On Thursday 30 April a sudden increase of the seismic activity accompanied the development of a third eruptive pulse. This last pulse produced an eruptive column raising up to 4 km above the crater and drifting southeast, affecting the Argentinean villages of El Bolson and Esquel (SERNAGEOMIN, 2015d). Finally, seismic and surface activities decreased gradually until 19 May, when SERNAGEOMIN lowered the alert level to orange and limited the exclusion zone to a distance of 10 km from the summit (SERNAGEOMIN, 2015e).

Throughout the entire eruptive period important events of fresh ash resuspension caused additional flight cancellations, road closures and respiratory issues given the fine nature (<10 μm) of the re-suspended material (Fig. 2e).

4. Tephra fallout deposits

In order to characterize the fallout deposit 35 samples were collected between 15 and 500 km from the volcano shortly after deposition (Fig. 3), thus ensuring that samples were pristine and unaffected by post-depositional hydrologic or aeolian remobilization. Amongst these, we used 13 samples for constraining model inputs (Table 1, samples between 15 and 500 km from the source) and 24 (of which we have deposit thickness information, Table 2) for model validation. In these points, the averaged deposit density was 997.3 kg/m^3 according to Romero et al. (2016). Optical and electronic

microscopic studies (SEM) revealed a dominant presence of brown blocky low to non-vesicular glassy fragments and subordinate white pumice clasts and cuspate glass shards (Figs. 4a and 4c). In addition, abundant plagioclase, orthopyroxene and clinopyroxene crystals and scarce lithic clasts were observed. Furthermore, electron microscope images show evidences of ash aggregation such as the presence of glass fragments (~100 μm) partially covered by very fine (< 10 μm) ash particles (coated particles *sensu* Brown et al., 2012) (Fig. 4a). Absolute density measured of medium-distal ash samples ranged between 2,300 and 2,700 kg/m^3. For grain-size analyses, samples were measured with a laser particle size analyser using a Horiba LA-960 apparatus (Table1). The results show a general bimodal grain size distribution for the samples located between 80 and 150 km from the vent (Fig. 4b). This is a common feature in many distal ash layers and has been attributed to premature fallout of fine ash aggregates due to the electrostatic charging and water vapour condensation in the eruption column (e.g. Brazier et al., 1983). In contrast, samples located beyond 200 km from the volcano have a grain size distribution tending to uni-modal, with an important population of fine ash (< 64 μm) (Fig. 4d). Similar complexities in distal ash fall layers were described for the 2008 Chaitén eruption and interpreted as a result of multiple deposit overlap and fine particle aggregation processes (Watt et al., 2009).

Preliminary bulk XRF chemical major element analysis of the ash collected at 100 km from the vent at Villa La Angostura was also carried out, reflecting a basaltic-andesitic composition. This is in agreement with findings by Romero et al. (2016) and Segura et al. (2015). However studies carried out by other authors reported low K andesitic composition (Astudillo et al., 2015) and andesitic composition (Bertin et al., 2015; Van Eaton et al., 2016) in the whole rock analysis. Juvenile material corresponds to medium K dacite (Astudillo et al., 2015; Bertin et al., 2015; Segura et al., 2015). Figure 5 shows the total alkali vs. silica plot including samples from previous eruptions for comparison.

5. Modelling Strategies

We ran the WRF/ARW-FALL3D-7.0 modelling system first in eruption mode from 22 April at 21:00 UTC to 1 May at 00:00 UTC (3 pulses) and then in resuspension mode up to 4 May at 00:00 UTC, using as potential resuspension source regions the fallout deposits obtained previously. In both cases, the meteorological driver was the WRF/ARW model configured as in the SHN-SMN experimental setup (Collini et al., 2013). The FALL3D computational domain spanned from 80°W to 48°W in longitude and from 48°S to 30°S in latitude, with horizontal spatial resolution of 0.2° and 20 vertical layers.

5.1. Eruption ash clouds

Eruption source parameters for FALL3D resemble the operational conditions (Table 3). Eruption column heights were taken from the SERNAGEOMIN reports derived from in situ observations and consist of 3 pulses (22, 23 and 30 April) ejecting material at 15, 15 and 4 km above the vent respectively. At this stage, the model ran with a Total Grain Size Distribution (TGSD) similar to that obtained by Scasso et al. (1994) for the 1991 Hudson eruption, assumed as representative of a sub-Plinian eruption style (Osores et al., 2011). This is the same TGSD that was used by the Buenos Aires VAAC over the entire eruptive period (Fig. 6a). However, a more realistic granulometry was considered once field data became available, allowing to reconstruct a TGSD (Fig. 6b) using the Voronoi Tessellation technique (Bonadonna and Houghton, 2005). Successive runs of FALL3D were made using the new granulometry discretized in 11 bins ranging from -1ϕ (2 mm) to 9ϕ (2 μm). A standard linear dependency of particle density with diameter was assumed. Based on laboratory analysis (density calculation by pycnometer and electron microscopic) density values from 2,300 to 2,700 kg/m^3 and particle sphericities from 0.7 to 0.9 were used. The total mass eruption rate was estimated from column height and hourly wind fields according to Degruyter and Bonadonna (2012), using a Suzuki (Suzuki, 1983) distribution for the vertical mass release with Suzuki parameters A=4 and L=5. The experimental operational FALL3D setup considers also the Ganser (1993) fit for particle terminal velocities and the CMAQ option to estimate grid-dependent horizontal diffusion. Since aggregates were identified in petrographic and electron~~ic~~ microscope observations (Fig. 4a), a percentage of 20% of fine material was assumed to aggregate on a single particle class of 125 μm and density of 200 kg/m^3. This density is typical of the type of aggregate present in the samples (Brown et al., 2012). Finally, the model was configured to overlap successive forecasts of 72 h using a re-start from the previous day results, i.e. to initialize each run with the deposit and airborne mass from the previous run.

5.2. Resuspension ash clouds

Volcanic ash deposited during the first days of the eruption was repeatedly re-suspended. Persistent dust sources in Patagonia are located between 38º and 48ºS in arid and semi-arid regions to the East of the Andes (Prospero et al., 2002). Typical features of the region, such as strong surface winds, low soil water content, and sparse vegetation cover, create favourable conditions for dust emission (e.g. Gaiero et al., 2003). Ha~~u~~dley et al. (2004) also attributed this phenomenon to the complex terrain, the super-adiabatic lapse rate of the troposphere below 850 Mb, and the presence of a long subsidence inversion around 1400-1600 m. Following an eruption, resuspension activity is increased as fresh unconsolidated ash deposits can be easily remobilised by wind. Resuspension of

volcanic ash in the Andean region of Patagonia is most frequently observed in austral spring and summer, when the prevailing westerly wind at middle and upper levels become stronger and gusts above 110 km/h are reported (Gassó and Stein, 2007).

In resuspension modelling, emission schemes for particle suspension and saltation must be considered. As wind speed at the surface increases, the onset of particle movement is determined by the saltating particles, the first ones to be activated by wind. The minimum friction velocity~~,~~ at which particles begin to move~~,~~ is the so-called static threshold friction velocity (Greeley and Iversen, 1987), and depends on physical properties of particles (size and density) and surface conditions (e.g. soil moisture). In the case of resuspension, the WRF/ARW model furnishes hourly friction velocities and soil moisture for the computation of emission fluxes in those regions blanketed with fallout deposits. In particular, we used the Shao (2001) emission scheme implemented in the FALL3D model (Folch et al., 2014) to calculate the horizontal saltation flux at each surface point (masked with the deposit) and considering the whole deposit granulometric range. In contrast, the vertical emission rate was calculated only for particles with diameters less than 150 μm (6 bins only). This diameter cut-off excludes larger particles from suspension, preventing from overestimation of re-suspended mass near the source and reducing the computational cost.

6. Results and v~~V~~alidation

In order to perform a semi-quantitative model validation, we visually compared TERRA and AQUA satellite MODIS retrievals with simulated mass column load. The MODIS sensor contains 36 spectral bands (from visible to thermal infrared) that collect data at three spatial resolutions of 250, 500, and 1~~,~~000 m. We used the thermal bands to calculate Brightness Temperature Differences (BTD; Prata, 1989) differentiating ash from meteorological clouds. Despite some well-known limitations of this methodology (e.g. ash detection uncertainties in presence of water vapour, clear desert areas, etc.), it has been demonstrated to be accurate in identifying large eruption clouds (Rose and Mayberry 2000). The images used for our validation are from 23 April at 14:13 UTC, 24 April at 14:56 UTC and 25 April at 14:01 UTC for TERRA, and from 25 April at 18:19 UTC, 30 April at 18:38 UTC, 2 May at 18:25 UTC, and 3 May at 19:08 UTC for AQUA. A comparison by visual inspection between FALL3D results and MODIS retrievals was performed.

6.1. Eruption modelling

Simulations considering granulometries GA (Hudson) and GB (Calbuco) predicted an initial cloud movement towards NE during the first hours following the first pulse, changing mildly to NW.

However, after some hours, noticeable differences appear between both sets of runs. The forecast considering GA shows a movement towards to NW, while for GB the cloud drifts to the North widening to West and to East but showing a leading NW direction (Figs. 7a and 7b). On 23 April the cloud reached Neuquén and other major cities, causing airport disruptions. Two main clouds are evident from the visible MODIS image at 14:13 UTC (Fig. 7c) and highlighted by the BTD algorithm (Fig. 7d). Simulations considering the granulometry GB clearly capture these two maxima (corresponding to different pulses) and show, as expected, a much better correlation with satellite imagery (Figs. 7b and 7d).

On 24 April the cloud reached Uruguay after crossing over Argentina. Observations at 15:00 UTC (Figs. 8c and 8d) show the cloud over the provinces of Buenos Aires, La Pampa, Córdoba, Mendoza and Santa Fe. Model results using GA (Fig. 8a) and GB (Fig. 8b) show a similar dispersion pattern but differ notably on the cloud extent and column mass load, with GB (Fig. 8b) having a much larger amount of ash over Buenos Aires, La Pampa and Chile. A displacement is observable between the maximum predicted by FALL3D and that observed over Santa Rosa city, being the forecast slightly southerly. On 30 April, when the third eruptive pulse occurred, the eruption cloud was observed by MODIS moving towards SE (Figs. 9c and 9d) over the provinces of Rio Negro and northern Chubut. Model results using GA (Fig. 9a) and GB (Fig. 9b) are similar in direction but, again, GB gives much higher mass values.

The erupted mass estimated according to Degruyter and Bonadonna (2012) differs in both cases. For GA, a total mass of 9.1×10^{11} kg was obtained for the first two pulses. In the simulations, a 99.72% of this mass was already deposited by April 25, and only a 0.26% remained airborne (the other 0.02% left the domain). In contrast, for GB, the total mass was of 7.4×10^{11} kg, with 75.16% deposited by April 25 (22.92% and 1.92% airborne and outside the domain respectively). For comparison, Romero et al. (2016) estimated a deposit mass of 2.8×10^{11} kg. These differences of a factor ~3 between simulations and field estimations are common and can be caused by a number of factors (e.g. Mastin et al., 2009). Figure 10 compares the simulated deposit thickness considering GA (Fig. 10b) and GB (Fig. 10c) with the isopachs map of Romero et al. (2016). The GB run shows a better agreement with Romero et al. (2016), although the model predicts two main northwest and east deposit axes, the later rotated with respect observations.

Finally, in order to have an additional quantitative validation, we compare deposit thicknesses at 24 locations (Romero et al., 2016; Table 2) with model results. The scatter plot is shown in Figure 11.

6.2. Resuspension modelling

During 2-3 May, ash was re-suspended within a N-S band East of Junín de Los Andes, where no rain had occurred since the beginning of the eruption and surface friction velocities were higher

than the threshold values. In our modelling strategy, we delineate the potential region for emission by looking at grid points with deposit mass loads exceeding 1.5 kg/m^2. This value was selected matching the emission region with satellite observations. We used the Shao emission scheme (Folch et al., 2014) with a threshold friction velocity between 0.4 and 0.8 m/s to obtain hourly emission mass fluxes (if any). Figure 12 shows, for illustrative purposes, the vertical mass flux at a particular time instant (3 May at 18 UTC). In contrast, Figure 13 gives the evolution in time of the total emission rate from 2 May at 00 UTC onwards (i.e. the total mass emitted per unit time). Note how three peaks are clearly visible during afternoons (at around 18:00 UTC, 15:00 LT), when surface heating increases atmospheric instability leading to more intense thermal turbulence and surface winds. The peaks of 2 and 3 May correspond to the events observed by MODIS (Figs. 14b, 14d and 14f). Eyewitnesses reported that the 3 May event was the most intense, in agreement with MODIS observations (Fig. 14f).

Figure 15 shows visibility observations at the Neuquén surface weather station from 2 to 5 May. As observed, visibility did not show any significant decrease during 2 May although ash in the atmosphere was reported (red circles from 2 May at 16:00 UTC to 3 May at 01:00 UTC). In contrast, during 3 May, volcanic ash observations clearly correlate with low visibility conditions (red circles from 13:00 UTC to 23:00 UTC) leading to a decrease down to 500 meters at 23:00 UTC. On May 2 at 18:25 UTC the MODIS image (Fig. 14b) shows a resuspension cloud NE of Calbuco and reaching Neuquén city, in good agreement FALL3D simulation (Fig. 14a). On 3 May a major resuspension event occurred E and NE of volcano. The cloud moved NE covering a large area and reaching the south of Santa Fe and Cordoba provinces (Fig. 14d and 14f). The FALL3D model forecast (Fig. 14c and 14e) predicted plume direction and shape (the modelled contour of 2.5 g/m^2 matches well the satellite images). The forecast predicted also the occurrence of a third resuspension event during 4 May, but this was not seen by MODIS, possibly because of the presence of meteorological clouds (the effect of cloud cover on surface heating could also explain a reduction of ash flux emission).

A remarkable eruption as the Calbuco volcano, lead to a substantial scientific, political, and media interest which decreases progressively. However, lessons learned from previous events indicate that the consequences of an eruption can persist for several years. A continued monitoring is required for a long-term volcanic hazard assessment and persistent efforts of the authorities to mitigate the impacts of volcanic crises.

7. Summary and conclusions

The experimental operational setup of the WRF/ARW-FALL3D-7.0 modelling system was validated during the Calbuco eruption and associated resuspension events. As in previous validation

cases (Folch et al., 2008; 2012; Collini et al., 2013; Osores et al., 2013) the model predicted ash cloud dispersion and ground deposition successfully. Model results were significantly enhanced when a reconstructed TGSD (GB) was used and the effects of aggregation considered. Regarding resuspension forecast, the model predicted well the occurrence and characteristics of the 2-3 May events.

These encouraging results have led us to consider transferring the use of FALL3D model into operations at the Buenos Aires VAAC. However, model input uncertainties can be large during an eruption. In the case of Calbuco only few geologic studies existed before the volcano erupted with little precursory activity. This highlights the importance of having a complete pre-defined database with expected model inputs for different scenarios that allow running a first early forecast. For this reason, researchers of the Argentinean SMN are compiling a database for all active volcanoes under the Buenos Aires VAAC responsibility (VORHISE; Farías et al., 2014). In addition, the "Ministerio de Ciencia Tecnología e Innovación Productiva" and the "Comisión de Trabajo de Gestión de Riesgos" (www.mincyt.gov.ar/ministerio/comision-de-trabajo-de-riego.html) are working on a volcanic ash sampling network and volcanic eruption protocols that can improve the assessment of crucial model inputs in near-real time. Moreover, transnational cooperation between Chile and Argentina is needed to exchange and extend data from active volcanoes.

Acknowledgements

This work used computational resources from CCAD – Universidad Nacional de Córdoba (http://ccad.unc.edu.ar/), in particular the Mendieta Cluster, which is part of SNCAD – MinCyT, República Argentina. The authors would like to thank to CONAE for provide MODIS images. We thank to Dra. Graciela Romero and Adriana Blanc for the use of Horiba LA-960 laser particle size analyzer to estimate grain size distribution of individual samples. The WRF/ARW modelling system ran in a cluster installed at the Servicio Meteorológico Nacional (SMN) of Argentina with funds from the Argentinean Project PIDDEF 41/10: "Pronóstico del tiempo para estudios de vulnerabilidad e impacto socioeconómico". We thank ~~to~~ Raul Rodano and Aerolineas Argentinas for the information about the impact of the Calbuco volcanic eruption in the rescheduling of flights. The authors acknowledge the editor Joan Martí and the reviews from two anonymous referees that improved the manuscript.

References

Astudillo, V., Bertin, L., and Bertin, D. (2015). Características texturales y composicionales de la tefra del ciclo eruptivo de Abril-Mayo de 2015 en el volcán Calbuco. In Congreso Geológico Chileno, No. XIV, La Serena, Chile.

Baxter, P.J. (1999). Impacts of eruptions on human health. In: Siggurdson, H. (Ed.), Encyclopedia of Volcanoes. Academic Press, New York, pp. 1035–1043.

Bertin, D, Amigo, A., Mella, M., Astudillo, V., Bertin, L., and Bucchi, F. (2015). Erupción del volcán Calbuco 2015: Estratigrafía eruptiva y volumen involucrado. In Congreso Geológico Chileno, No. XIV, La Serena, Chile.

Bonadonna, C., and Houghton, B. F. (2005). Total grain-size distribution and volume of tephra-fall deposits. Bulletin of Volcanology, *67*(5), 441-456.

Brazier, S., Sparks, R. S. J., Carey, S. N., Sigurdsson, H., and Westgate, J. A. (1983). Bimodal grain size distribution and secondary thickening in air-fall ash layers. Nature, 301 (5896), 115-119.

Brown, R. J., Bonadonna, C., and Durant, A. J. (2012). A review of volcanic ash aggregation. Physics and Chemistry of the Earth, Parts A/B/C, 45, 65-78.

Casadevall, T.J. (1993). Volcanic hazards and aviation safety, lessons of the past decade. Flight Safety Foundation – Flight Safety Digest, 1-9 May 1993.

Clavero, J., Godoy, E., Arancibia, G., Rojas, C., and Moreno, H. (2008). Multiple Holocene sector collapses at Calbuco volcano, Southern Andes. Abstracts, Poster Session III, IAVCEI General Assembly, Reykjavik, Iceland, p. 41.

Collini, E., Osores, M. S., Folch, A., Viramonte, J. G., Villarosa, G., and Salmuni, G. (2013). Volcanic ash forecast during the June 2011 Cordón Caulle eruption. Natural hazards, 66(2), 389-412.

Costa, A., Macedonio, G., and Folch, A. (2006). A three-dimensional Eulerian model for transport and deposition of volcanic ashes. Earth and Planetary Science Letters, 241(3), 634-647.

Degruyter, W., and Bonadonna, C. (2012). Improving on mass flow rate estimates of volcanic eruptions. Geophysical Research Letters, 39 (16).

Draxler, R. R., and Hess, G. D. (1998). An overview of the HYSPLIT_4 modelling system for trajectories. Australian Meteorological Magazine, 47(4), 295-308.

Farias C. P., Collini E. A., Viramonte J. G. and Ortiz Guerrero N. (2014). Base de Datos Regional de Volcanes que se encuentran en el dominio del Centro de Avisos de Ceniza Volcanica (VAAC) Buenos Aires. In XIX Congreso Geológico Argentino, Simposio: Volcanismo de los Andes - Tectónica y Volcanismo. Actas: i. (pp. 1832-1833). Córdoba, Argentina.

Folch, A., Jorba, O., and Viramonte, J. (2008). Volcanic ash forecast application to the May 2008

Chaitén eruption. Natural Hazards and Earth System Sciences, 8, 927-940.

Folch, A., Costa, A., and Macedonio, G. (2009). FALL3D: A computational model for transport and deposition of volcanic ash. Computers & Geosciences, 35(6), 1334-1342.

Folch, A., Costa, A., and Basart, S. (2012). Validation of the FALL3D ash dispersion model using observations of the 2010 Eyjafjallajökull volcanic ash clouds. Atmospheric Environment, 48, 165-183.

Folch, A., Mingari, L., Osores, M. S., and Collini, E. (2014). Modeling volcanic ash resuspension. Natural Hazards and Earth System Sciences, 14(1), 119.

Gaiero, Diego M., J-L. Probst, Pedro J. Depetris, Susana M. Bidart, and Lydia Leleyter. (2003). Iron and other transition metals in Patagonian riverborne and windborne materials: geochemical control and transport to the southern South Atlantic Ocean. Geochimica et Cosmochimica Acta 67(19). 3603-3623.

Ganser, G. H. (1993). A rational approach to drag prediction of spherical and nonspherical particles. Powder Technology, 77(2), 143-152.

Gassó, S. and Stein A.F. (2007). Does dust from Patagonia reach the sub-Antarctic Atlantic Ocean? Geophysical Research Letters 34(1).

Greeley, R., and Iversen, J. D. (1987). Wind as a geological process: on Earth, Mars, Venus and Titan (Vol. 4). CUP Archive.

Guffanti, M., Mayberry, G. C., Casadevall, T. J., and Wunderman, R. (2009). Volcanic hazards to airports. Natural hazards, 51(2), 287-302.

Hadley, D., Hufford, G. L., and Simpson, J. J. (2004). Resuspension of Relic Volcanic Ash and Dust from Katmai: Still an Aviation Hazard, Weather and forecasting, 19, 829-840.

Hickey-Vargas, R., Abdollahi, M.J., Parada, M.A., López-Escobar, L. & Frey, F.A. (1995). Crustal xenoliths from Calbuco Volcano, Andean Southern Volcanic Zone: implications for crustal composition and magma-crust interaction. Contributions to Mineralogy and Petrology, 119, 331-344.

Johnston, D., Dolan, L., Becker, J., Alloway, B., and Weinstein, P. (2001). Volcanic ash review—Part 1: impacts on lifelines services and collection/disposal issues. Auckland Regional Council Technical Publication, 144, 50.

Lahsen, A., Moreno, H., Varela, J., Munizaga, F., and López, L. (1985). Geología y riesgo volcánico del volcán Calbuco y centros eruptivos menores. Proyecto Canutillar. Universidad de Chile.

Le Bas, M. J., Le Maitre, R. W., Streckeisen, A., and Zanettin, B. (1986). A chemical classification of volcanic rocks based on the total alkali-silica diagram. Journal of petrology, 27(3), 745-750.

Lopez-Escobar, L., Parada, M. A., Moreno, H., Frey, F. A., and Hickey-Vargas, R. L. (1992). A contribution to the petrogenesis of Osorno and Calbuco volcanoes, Southern Andes (41° 00'-41° 30'S): comparative study. Andean Geology, 19(2), 211-226.

Mastin, L. G., Guffanti, M., Servranckx, R., Webley, P., Barsotti, S., Dean, K., Durant, A., Ewert, J. W., Neri, A., Rose, W. I., Schneider, D., Siebert, L., Stunder, B., Swanson, G., Tupper, A., Volentik, A., and Waythomas, C. F. (2009). A multidisciplinary effort to assign realistic source parameters to models of volcanic ash-cloud transport and dispersion during eruptions. Journal of Volcanology and Geothermal Research, 186(1), 10-21.

Mella, M., Moreno, H., Vergés, A., Quiroz, D., Bertin, L., Basualto, D., Bertin, D. & Garrido, N. (2015). Productos volcánicos, impactos y respuesta a la emergencia del ciclo eruptivo abril-mayo (2015) del volcán Calbuco. In Congreso Geológico Chileno, No. XIV, La Serena, Chile.

Moreno, H. (1974). Airplane flight over active volcanoes of central-south Chile. In Int. Symp. Volcanol. (p. 56). Univ. Chile.

Moreno, H. (1976). The Upper Cenozoic volcanism in the Andes of Southern Chile (Irom 40 00'to 41 30'S. L.). In Symposium on Andean and Antarctic Volcanology Problems, Intearnational Association (pp. 143-173).

Munizaga, F., Hervé, F., Drake, R., Pankhurst, R. J., Brook, M., and Snelling, N. (1988). Geochronology of the Lake Region of south-central Chile (39–42 S): preliminary results. Journal of South American Earth Sciences, 1(3), 309-316.

Osores S., Pujol G., Collini E., and Folch A. (2011). Análisis de la dispersión de ceniza volcánica en la atmósfera modelada por el FALL3D para la erupción del volcán Hudson en 1991. Conferencia Geográfica Regional (UGI), Chile

Osores, M. S., Folch, A., Collini, E., Villarosa, G., Durant, A., Pujol, G., and Viramonte, J. G. (2013). Validation of the FALL3D model for the 2008 Chaitén eruption using field and satellite data. Andean Geology, 40(2), 262-276.

Parada, M., Godoy, E., Hervé, F., and Thiele, R. (1987). Miocene calcalkaline plutonism in the Chilean Southern Andes. Revista Brasileira de Geosciéncias, 17(4), 450-455.

Prata, A. J. (1989). Infrared radiative transfer calculations for volcanic ash clouds. Geophysical research letters, 16(11), 1293-1296.

Prospero, Joseph M., Paul Ginoux, Omar Torres, Sharon E. Nicholson, and Thomas E. Gill. (2002). Environmental characterization of global sources of atmospheric soil dust identified with the Nimbus 7 Total Ozone Mapping Spectrometer (TOMS) absorbing aerosol product. Reviews of geophysics, 40(1).

Romero J. E., Morgavi D., Arzilli F., Daga R., Caselli A., Reckziegel F., Viramonte J., Díaz-

Alvarado J., Polacci M., Burton M., and Perugini D. (2016). Eruption dynamics of the 22-23 April 2015 Calbuco Volcano (Southern Chile): Analysis of tephra fall deposits. Journal of Volcanology and Geothermal Research, 317, 15-29.

Rose, W. I., and Mayberry, G. C. (2000). Use of GOES thermal infrared imagery for eruption scale measurements, Soufriere Hills, Montserrat. Geophysical research letters, 27(19), 3097-3100.

Scasso, R. A., Corbella, H., and Tiberi, P. (1994). Sedimentological analysis of the tephra from the 12–15 August 1991 eruption of Hudson volcano. Bulletin of Volcanology, 56(2), 121-132.

Segura, A., Castruccio, A., Clavero, J., Le Pennec JL., Roche, O., Samaniego, P., Droguetti, B., and Romero, J. (2015). Fallout deposits of the 22-23 April 2015 eruption of Calbuco volcano, Southern Andes. In Congreso Geológico Chileno, No. XIV, La Serena, Chile.

Sellés, D. and Moreno, H., (2011). Geología del volcán Calbuco, Región de los Lagos. Servicio Nacional de Geología y Minería, Carta Geológica de Chile, Serie Geología Básica, No. XX, 30 p., 1 mapa escala 1:50.000, Santiago

Stern, C. (2004). Active Andean volcanism: its geologic and tectonic setting. Revista Geológica de Chile, 31(2), 161-206.

SERNAGEOMIN (2015a). Reporte Especial de Actividad Volcánica (REAV) Región de los Lagos. (REAV) Año 2015 Abril 22 (20:45 HL)

SERNAGEOMIN (2015b). Reporte Especial de Actividad Volcánica (REAV) Región de los Lagos. Año 2015 Abril 22 (22:30 HL).

SERNAGEOMIN (2015c). Reporte Especial de Actividad Volcánica (REAV) Región de los Lagos. Año 2015 Abril 23 (10:30 HL).

SERNAGEOMIN (2015d). Reporte de Actividad Volcánica (RAV) Región de los Lagos. Año 2015 Abril 30 (15:00 HL).

SERNAGEOMIN (2015e). Reporte de Actividad Volcánica (RAV) Región de los Lagos. Año 2015 May 19 (11:00 HL).

Shao, Y. (2001). A model for mineral dust emission. Journal of Geophysical Research: Atmospheres (1984–2012), 106(D17), 20239-20254.

Suzuki, T. (1983). A theoretical model for dispersion of tephra. Arc volcanism: physics and tectonics, 95, 113.

Thiele, R.; Godoy, E.; Francisco, H.; Parada, M.A.; and Varela, J. (1985). Estudio geológico-estructural regional y tectónico del área Petrohué-Canutillar. Informe del Departamento de Geología y Geofísica de la Universidad de Chile para Endesa (Inédito), proyecto Canutillar: 157 p.

Van Eaton, A.R., Amigo, A., Bertin, D., Mastin, L.G., Giacosa, R.E., González, J., Valderrama, O., Fontijn, K., and Behnke, S.A. (2016). Volcanic lightning and plume behavior reveal evolving hazards during the April 2015 eruption of Calbuco volcano, Chile. Geophysical Research Letters, 43.

Watt, S. F., Pyle, D. M., Mather, T. A., Martin, R. S., and Matthews, N. E. (2009). Fallout and distribution of volcanic ash over Argentina following the May 2008 explosive eruption of Chaitén, Chile. Journal of Geophysical Research: Solid Earth (1978–2012), 114(B4).

Wilson, T. M., Cole, J. W., Stewart, C., Cronin, S. J., and Johnston, D. M. (2011). Ash storms: impacts of wind-remobilised volcanic ash on rural communities and agriculture following the 1991 Hudson eruption, southern Patagonia, Chile. Bulletin of Volcanology, 73(3), 223-239.

Witham, C. S., Hort, M. C., Potts, R., Servranckx, R., Husson, P., and Bonnardot, F. (2007). Comparison of VAAC atmospheric dispersion models using the 1 November 2004 Grimsvötn eruption. Meteorological Applications, 14(1), 27-38.

Figure captions

Figure 1. (a) Location of Calbuco volcano. The red square shows the extent of the geological map. Volcanic Zones were included in South America map (lower left corner): NVZ: North Volcanic Zone, CVZ: Central Volcanic Zone, SVZ: Southern Volcanic Zone; AVZ: Austral Volcanic Zone. **(b)** Geological map of Calbuco volcano after Sélles and Moreno (2011). References: Pzm: Upper Palaeozoic meta-sedimentary rocks; Mg(t): Neogene tonalites; Mg(d): Neogene diorites; Mg(g): Neogene granites; Plhh: Early Pleistocene volcanic and volcano-clastic sequences; Plc1: Calbuco 1, Middle-Upper Pleistocene, basaltic-andesite lava flows with volcanoclastic deposits interbedded; Plc2: Calbuco 2, Upper Pleistocene, lava flows and pyroclastic rocks; Pldp2: Calbuco 2, Upper Pleistocene, flow and fall pyroclastic deposits; Plav2: Calbuco 2, Upper Pleistocene, volcanic avalanche deposits; Hc3: Calbuco 3, Upper Pleistocene-Holocene , lava flows interbedded with breccia and tuffs; Hap3: Calbuco 3, Upper Pleistocene-Holocene, Alerce ignimbrite and volcanoclastic deposits; Hdp3: Calbuco 3, Upper Pleistocene-Holocene, undifferentiated pyroclastic deposits; Hlp3: Calbuco 3, Upper Pleistocene-Holocene, lahars and pre-historic pyroclastic flows; Hc4, Calbuco 4, Holocene, dome-cone and associated lava flows. Others Holocene deposits: Hl4: recent and historic lahars; Plm: moraines; Plfg: fluvioglacial deposits; Hfa: ancient fluvial deposits; Hf recent fluvial deposits; Hlp marsh and lacustrine deposits; Hm: recent moraines; Ha: alluvial deposits; Hpl: recent playa lake deposits and Hc: colluvial deposits.

Figure 2. (a) Eruptive column during the first pulse (~15 km high). Photograph taken by an amateur photographer (https://500px.com) 14 minutes after the eruption start. **(b)** Aerial view of the eastern flank of Calbuco volcano showing pyroclastic density current deposits formed during pulses 1 and 2 (from SERNAGEOMIN webpage). **(c)** Roof collapse by fallout deposits at Ensenada, 15 km N from the volcano (from http://www.24horas.cl). **(d)** Junín de Los Andes covered by distal ash fallout on Thursday 23 April (from http://diadelsur.com). **(e)** resuspended ash over Bariloche (from www.lanacion.com.ar).

Figure 3. Location of deposit thickness sampled points (white points, used for model validation), and points with granulometric information (green points, used to reconstruct the TGSD GB). C: Calbuco Volcano; PM: Puerto Montt; VLA: Villa La Angostura; SCB: San Carlos de Bariloche; N: Neuquén; GR: General Roca.

Figure 4. Textural features and grain size distributions for samples representative of distal fallout. **(a-b)** Sample located at ~100 km from the vent showing evidence of ash aggregation (coated particles sensu Brown et al., 2012) and a bimodal grain size distribution. **(c-d)** Sample located at

~200 km from the vent showing a predominance of very fine ash and a grain size distribution tending to uni-modal.

Figure 5. TAS Classification (Le Bas et al., 1986) from bulk major element XRF geochemistry of distal ash deposits from the 2015 Calbuco eruption. Samples from previous eruptions are shown for comparison.

Figure 6. (a) TGSD (GA) used in experimental operational mode. **(b)** Reconstructed TGSD (GB) used in the simulations.

Figure 7. (a) Forecasted ash cloud column mass (g/m^2) for 23 April at 14:00 UTC considering granulometry GA (Fig. 6a). The inner red frame indicates the extent of the MODIS image. The black line indicates the 5 g/m^2 contour. **(b)** Same using granulometry GB (Fig. 6b). **(c)** True color image from TERRA-MODIS on 23 April at 14:13 UTC. **(d)** Brightness Temperature Difference (BTD). The yellow dashed line indicates the extension of the ash cloud, marked by visual inspection. C: Calbuco Volcano; PM: Puerto Montt; VLA: Villa La Angostura; SCB: San Carlos de Bariloche; N: Neuquén; GR: General Roca; SR: Santa Rosa; BB: Bahía Blanca; BA: Buenos Aires.

Figure 8. Same as in Figure 7 but for 24 April at 14:56 UTC.

Figure 9. Same as in Figure 7 but for 30 April at 19:00 UTC.

Figure 10. Deposit thickness. **(a)** Isopachs map after Romero et al. (2016). **(b)** Forecasted isopach map considering granulometry GA (Fig. 6a) on April 25 at 00:00 UTC. The black line indicates the 0.05 cm contour. **(c)** Same using granulometry GB (Fig. 6b). C: Calbuco Volcano; PM: Puerto Montt; VLA: Villa La Angostura; SCB: San Carlos de Bariloche; N: Neuquén; GR: General Roca; SR: Santa Rosa; BB: Bahía Blanca; BA: Buenos Aires.

Figure 11. Comparison between measured and computed deposit thickness (cm).

Figure 12. Mass flux of resuspension (ash emission rate) on May 3 at 18:00 UTC using the Shao emission scheme. . C: Calbuco Volcano; PM: Puerto Montt; VLA: Villa La Angostura; SCB: San Carlos de Bariloche; N: Neuquén; GR: General Roca; SR: Santa Rosa; BB: Bahía Blanca; BA: Buenos Aires.

Figure 13. Evolution in time of the total emission rate (integrated over the deposit) using ~~for~~ the Shao emission scheme.

Figure 14. Resuspension forecast. **(a)** Predicted column mass (g/m^2) on 2 May at 18:00 UTC. The inner red frame indicates the extent of the MODIS counterpart image. The black line indicates the 5 g/m^2 contour. **(b)** True color image from AQUA-MODIS at 18:25 UTC. Yellow dash line indicates the extent of the re-suspended ash, marked by visual inspection. **(**c**)** Predicted column mass (g/m^2) on 3 May at 15:00 UTC. **(d)** True color image from AQUA-MODIS at 14:51 UTC. **(e)** Predicted column mass (g/m^2) on 3 May at 19:00 UTC. **(f)** True color image from AQUA-MODIS at 19:08 UTC. C: Calbuco Volcano; PM: Puerto Montt; VLA: Villa La Angostura; SCB: San Carlos de Bariloche; N: Neuquén; GR: General Roca; SR: Santa Rosa; BB: Bahía Blanca; BA: Buenos Aires.

Figure 15. Visibility inferred from total suspended particle concentration at the Neuquén surface weather station.

Table captions

Table 1: Grain Size Distribution of sample points used to reconstruct the TGSD (Green points in Figure 3).

Table 2: Deposited Thickness of 24 sample points. Measured and Modelled by FALL3D (White points in Figure 3).

Table 3: Parameters used to run the FALL3D in experimental operational mode.

Table 1

Point Location			Grainsize class (ϕ). Weight in %.											
Name	**Lat**	**Lon**	**-1**	**0**	**1**	**2**	**3**	**4**	**5**	**6**	**7**	**8**	**9**	**Date**
T1	-41.2071	-72.5399	36.19	59.79	3,147	0.286	0.286	0.286	0	0	0	0	0	5/6/2015
T2	-41.2029	-72.5384	29,533	68.8	0.518	0.518	0.259	0.26	0	0	0	0	0	5/6/2015
T3	-40.7119	-71.9443	0	0	1,973	40,639	49.12	1,228	0	0	0	0	0	4/22/2015
T4	-41.1301	-71.4022	0	0	0	1,261	62,327	19,444	0.99	2,614	6,541	6,487	0.34	4/27/2015
T5	-40.8551	-71.5169	0	0	0.335	22,458	58.82	3,471	0.662	3,297	7,104	3,353	0.501	4/28/2015
T6	-40.7424	-71.6621	0	0	1,039	29,558	55,686	2,849	0	2,109	4,687	3,786	0.286	4/22/2015
T7	-40.1249	-71.2489	0	0	0	0.992	36,653	23,814	3,759	10.92	15.54	8,181	0.146	4/29/2015
T8	-39.7531	-71.1154	0	0	0	0.419	6,213	20.07	20,867	29,241	16,656	6,195	0.338	5/11/2015
T9	-39.9790	-70.7571	0	0	0	0.481	5,518	16.08	20,601	33,489	17,996	5,699	0.139	5/11/2015
T10	-39.9837	-71.0835	0	0	0	0.423	8,114	16,972	14,783	31.93	20,567	6.92	0.291	5/11/2015
T11	-39.9837	-71.0841	0	0	0	1,127	8,411	15,612	14,236	31,838	21,063	7,381	0.332	4/29/2015
T12	-39.9980	-70.8352	0	0	0	0.309	3,314	12,002	16,994	34.29	22,934	9,413	0.744	4/29/2015
T13	-39.0333	-67.5833	0	0	0	0	94,812	23,586	0	22,731	22,381	0	83.64	4/23/2015

Table 2

Points	Longitude	Latitude	Measured Thickness (cm)	Modeled Thickness (cm)
c1	-40.7631	-71.6401	0.2	0.30
c2	-39.0333	-67.5833	0.01	0.06
c3	-40.1304	-72.3862	0.01	0.02
c4	-38.9422	-72.0276	0.05	0.06
c5	-40.3224	-72.4813	0.05	0.01
c6	-40.4177	-72.7876	0	0.00
c7	-41.4718	-72.9365	0.01	0.05
c8	-39.3587	-71.5871	0.02	0.08
c9	-38.0715	-70.6131	0.01	0.05
c10	-37.8676	-71.0523	0.01	0.05
c11	-40.1551	-71.3542	0.5	0.15
c12	-39.1010	-67.5773	0.01	0.06
c13	-38.9533	-68.0676	0.01	0.07
c14	-40.0510	-70.0834	0.2	0.21
c15	-40.7285	-71.8087	0.5	0.16
c16	-40.7251	-71.7826	0.5	0.17
c17	-40.7123	-71.7903	0.4	0.16
c18	-40.0864	-71.1365	0.02	0.18
c19	-40.2202	-71.3624	0.4	0.15
c20	-40.4901	-71.5992	0.2	0.15
c21	-40.6293	-71.6617	0.2	0.17
c22	-40.7956	-71.5926	0.2	0.25
c23	-40.7812	-71.6618	0.3	0.23
c24	-40.8397	-71.5399	0.2	0.29

Table 3

Input parameter	Value
Model used to estimate total mass eruption rate	Degruyter and Bonadonna (2012)
Vertical mass distribution	Suzuki (1983)
Suzuki parameters	A=4, L=5
Particle terminal velocity	Ganser (1993)
Horizontal Diffussion	CMAQ
Aggregates	none
Initial grain size	-1ϕ to 8ϕ
Particle sphericity	0.9
Density range	900-1500 kg/m3

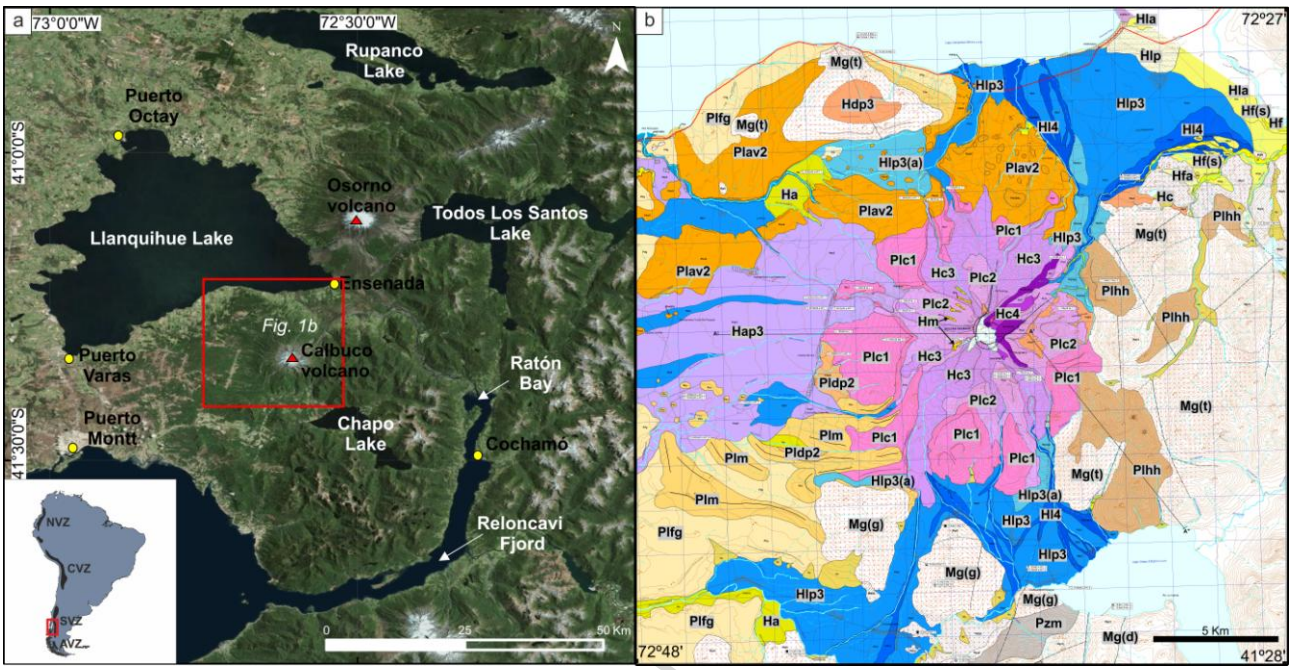

Fig. 1

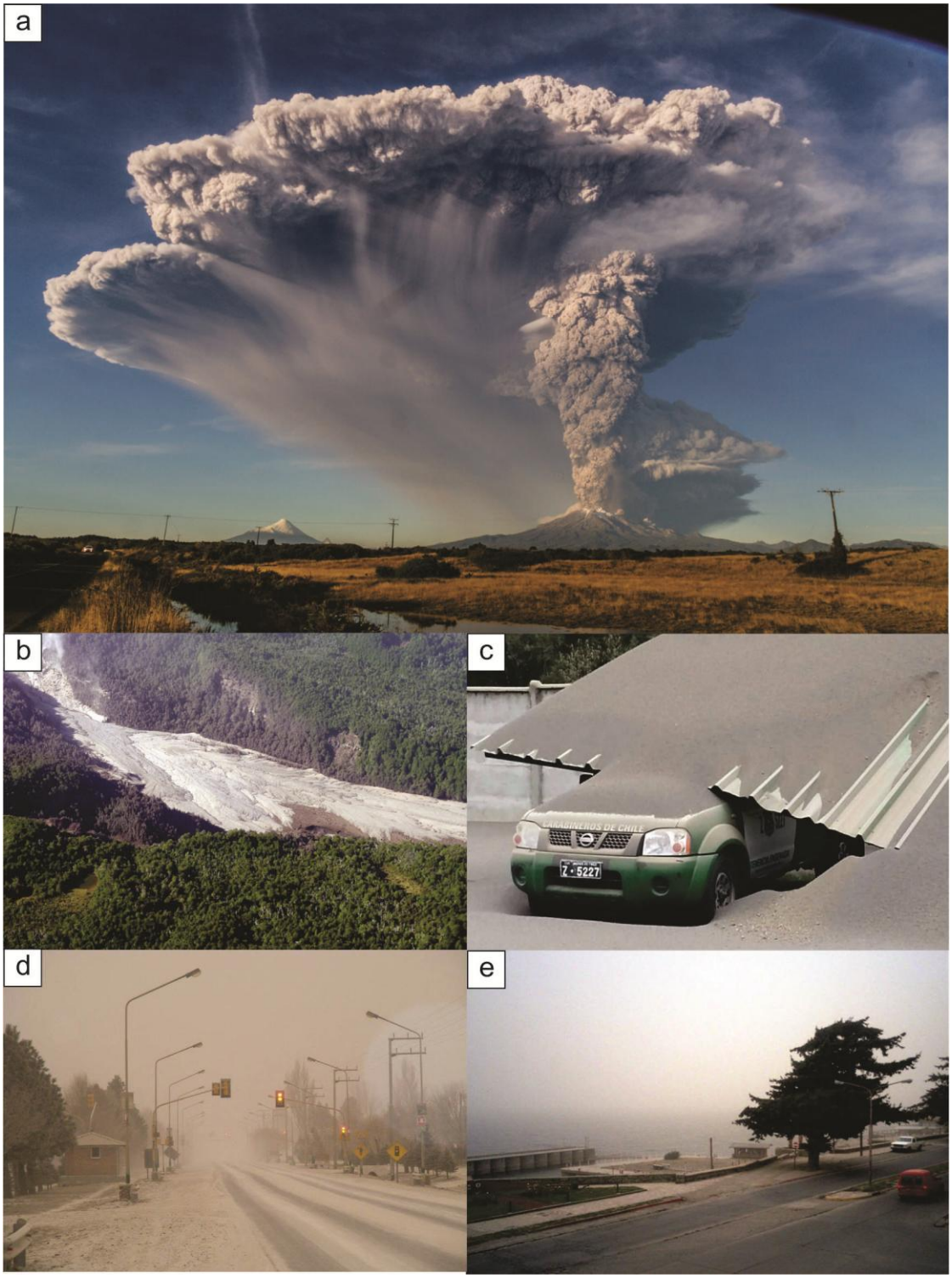

Fig. 2

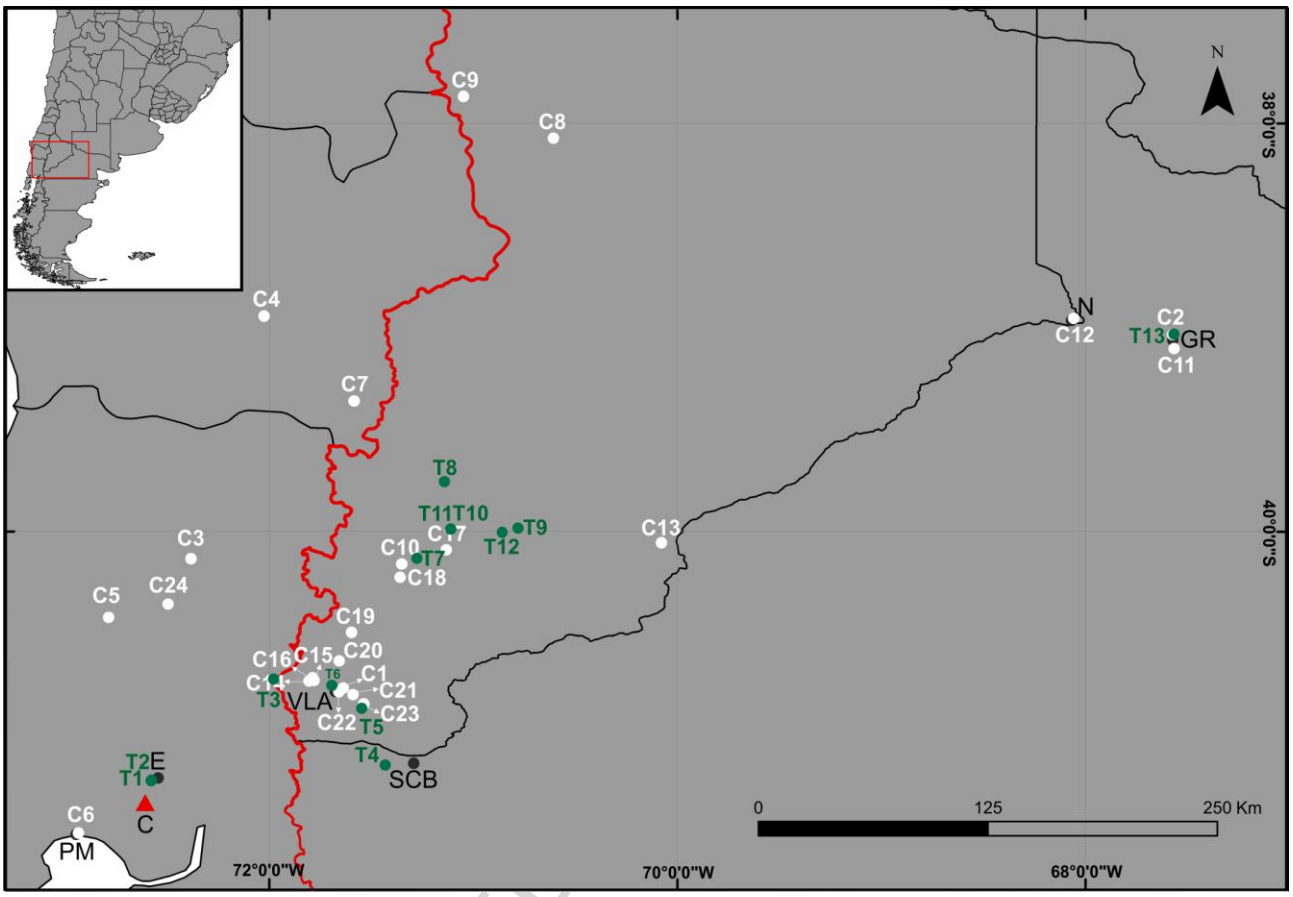

Fig. 3

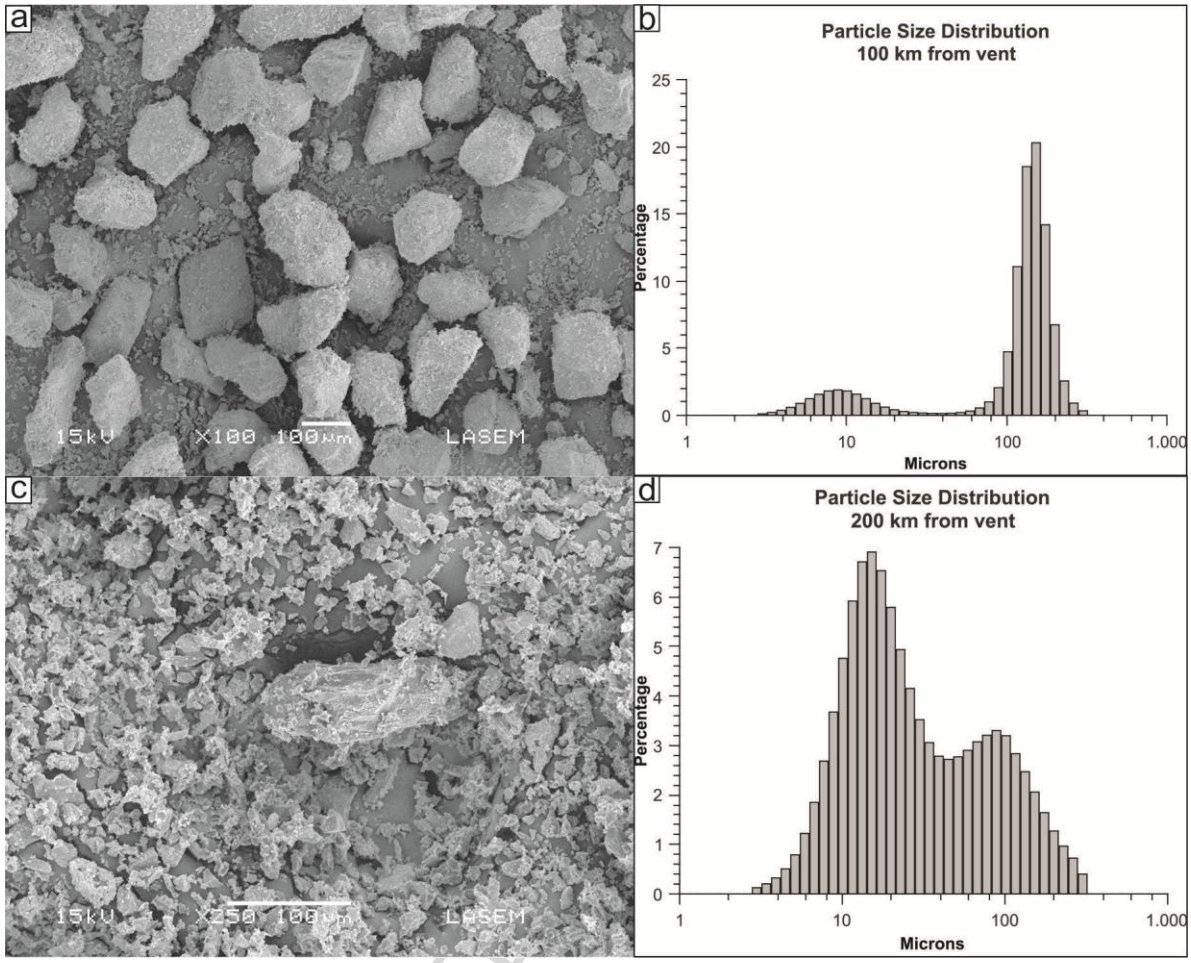

Fig. 4

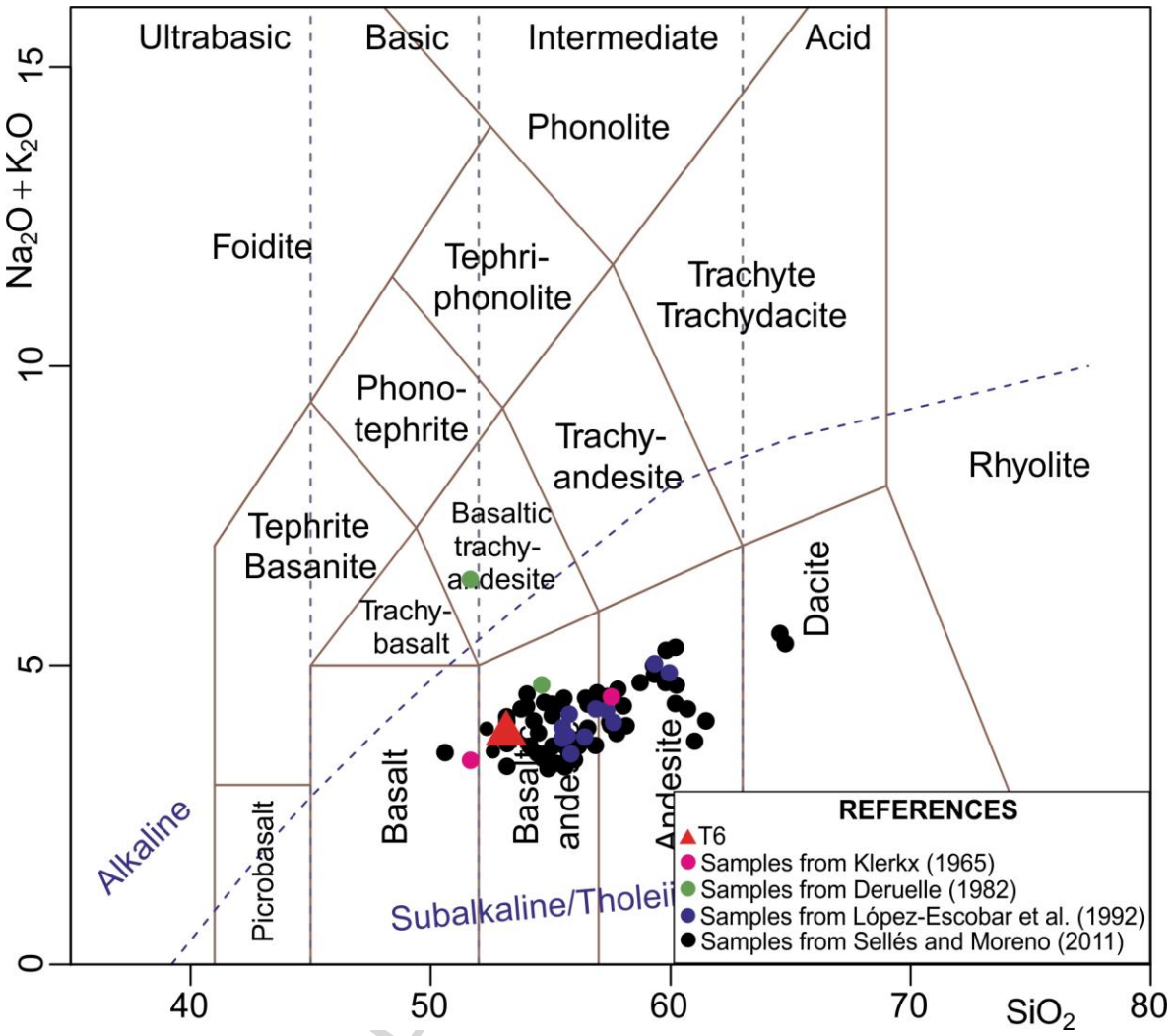

Fig. 5

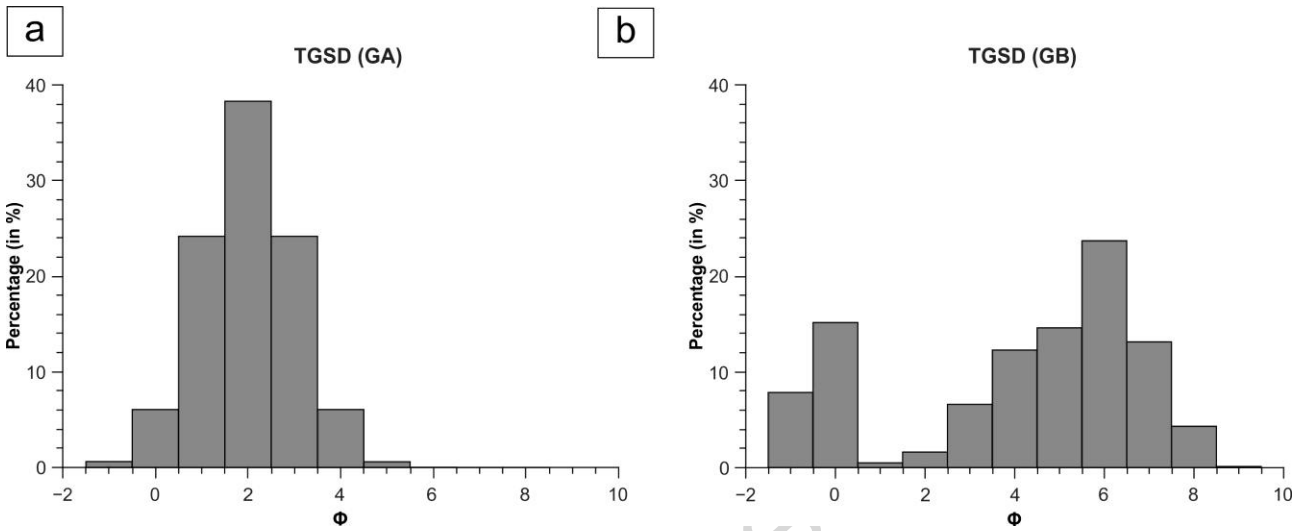

Fig. 6

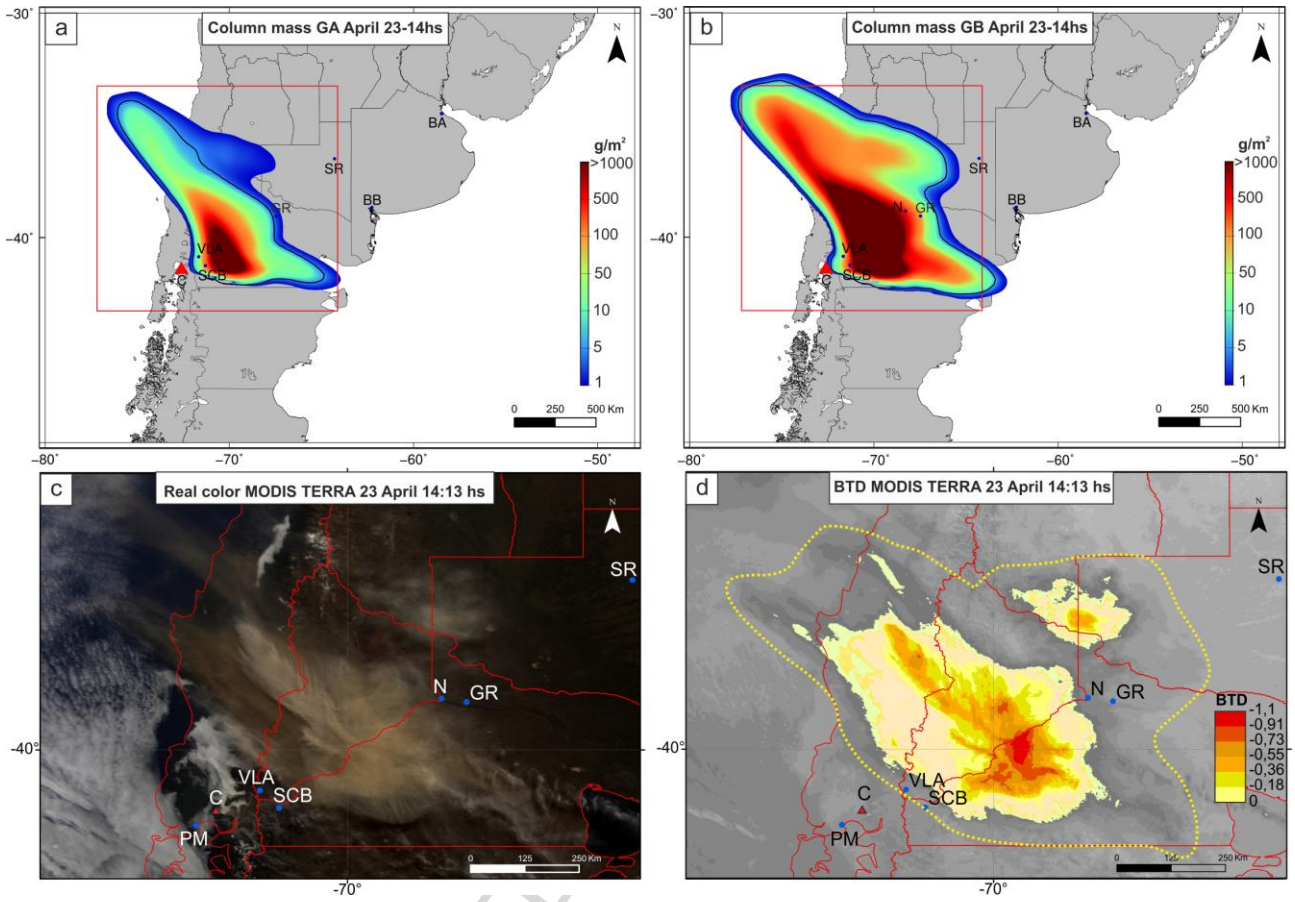

Fig. 7

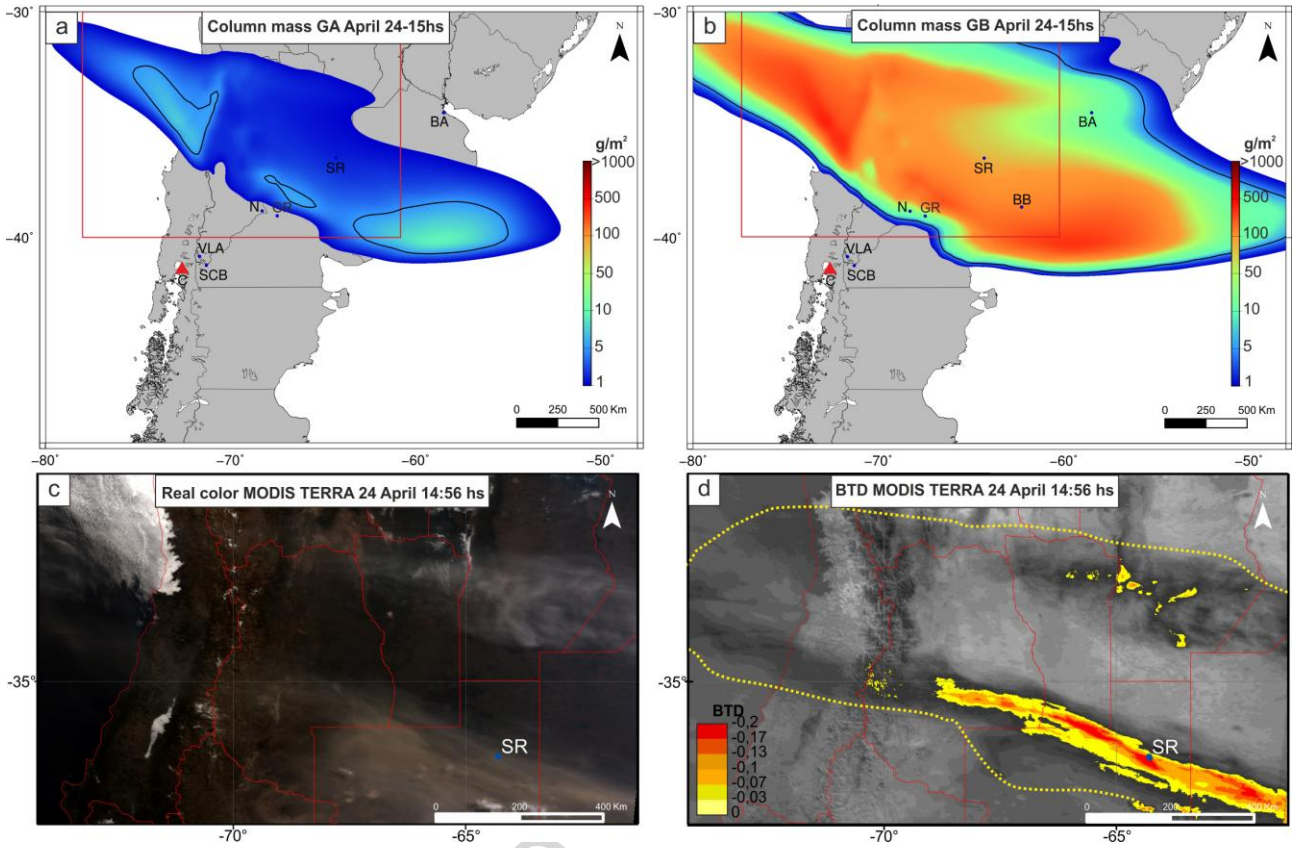

Fig. 8

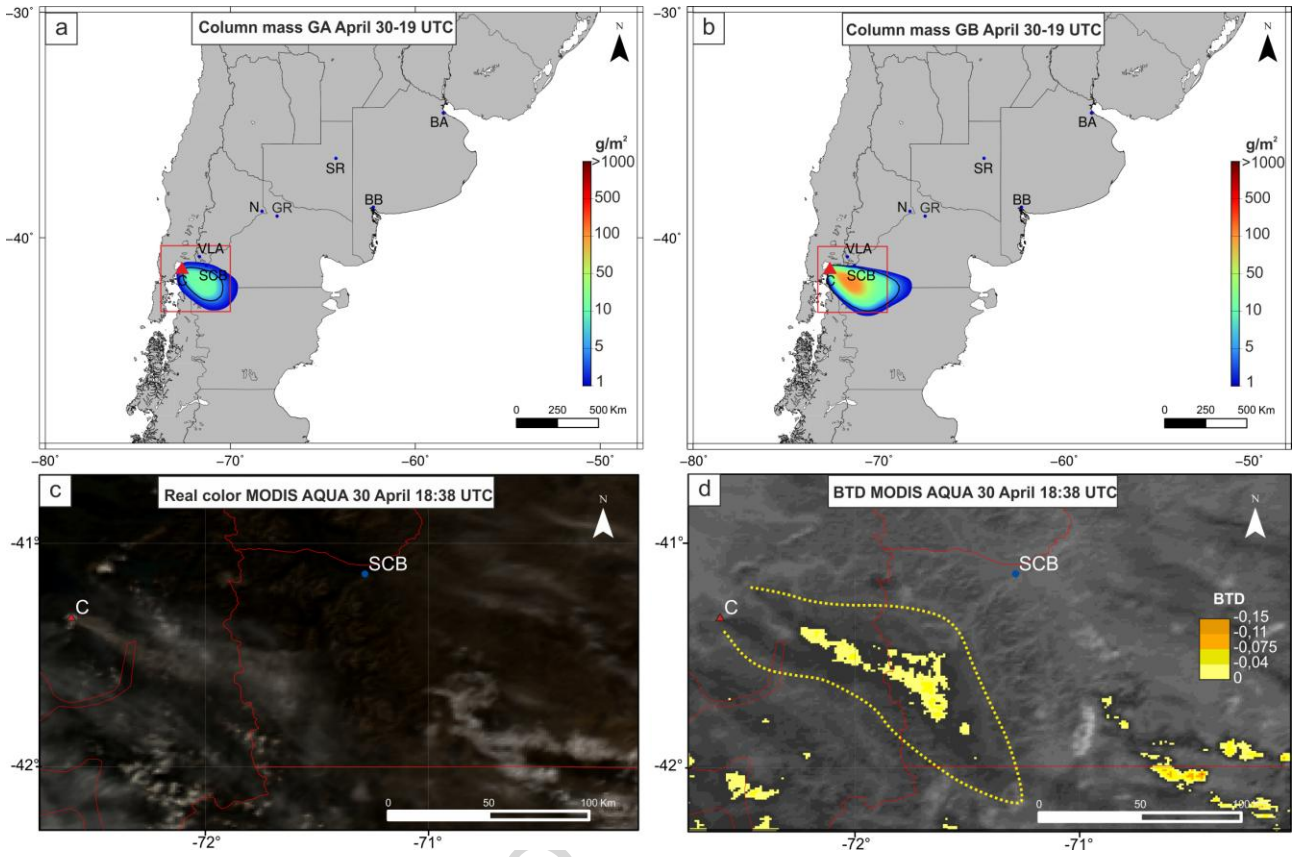

Fig. 9

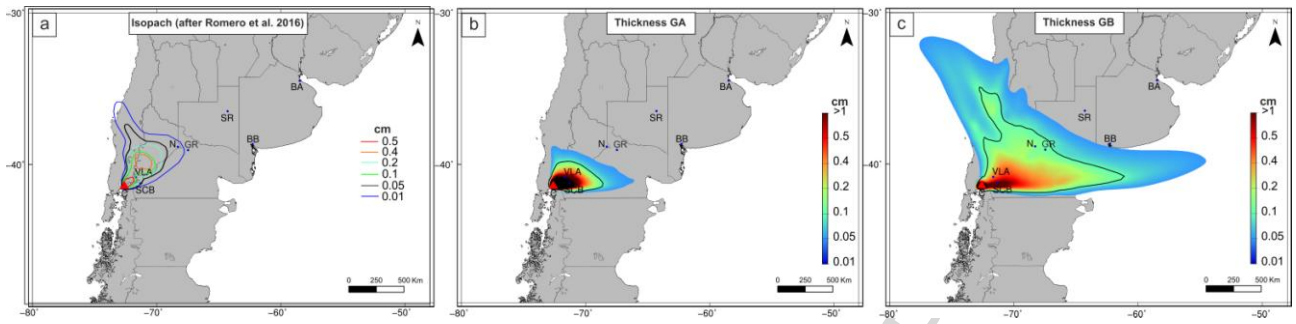

Fig. 10

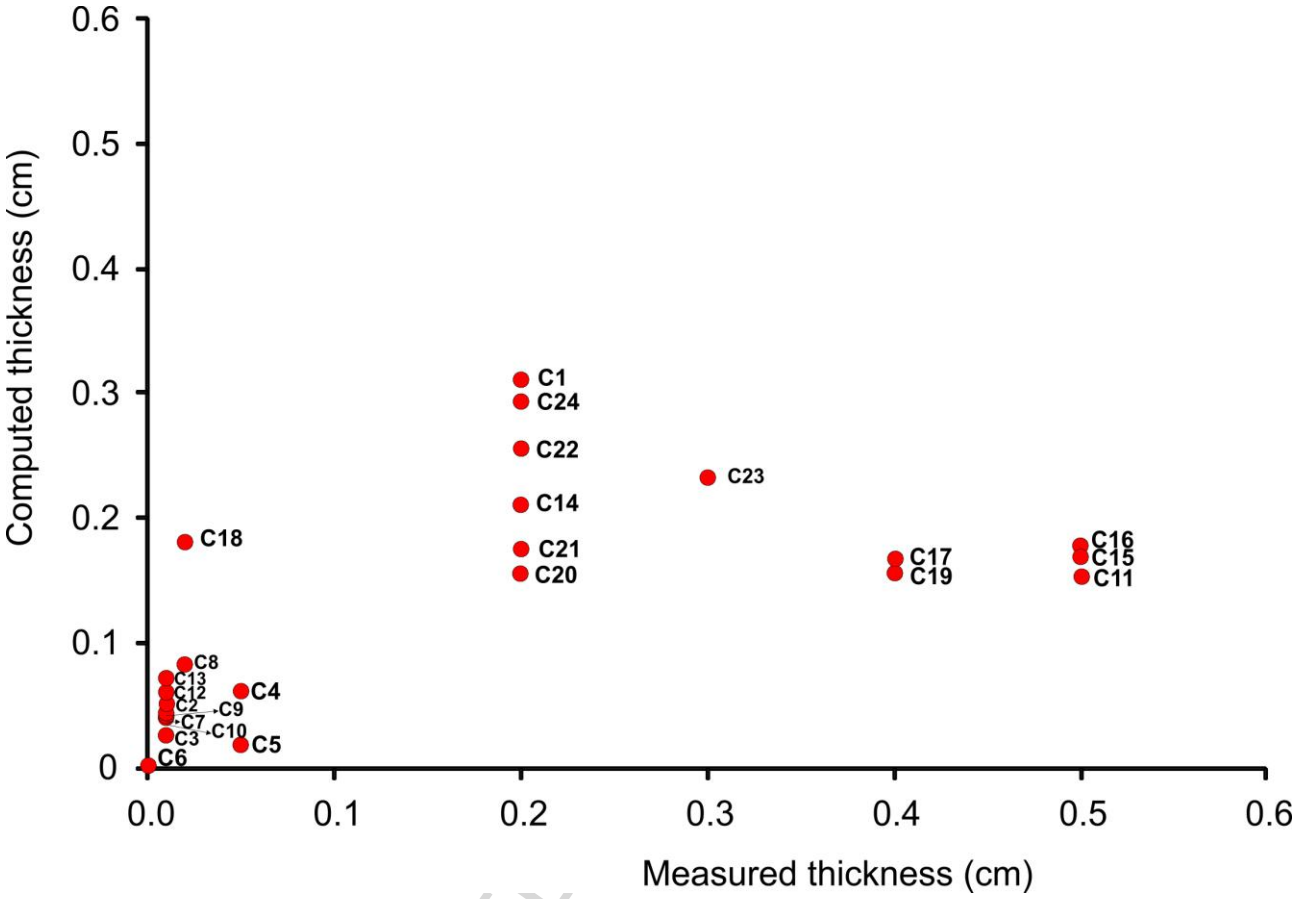

Fig. 11

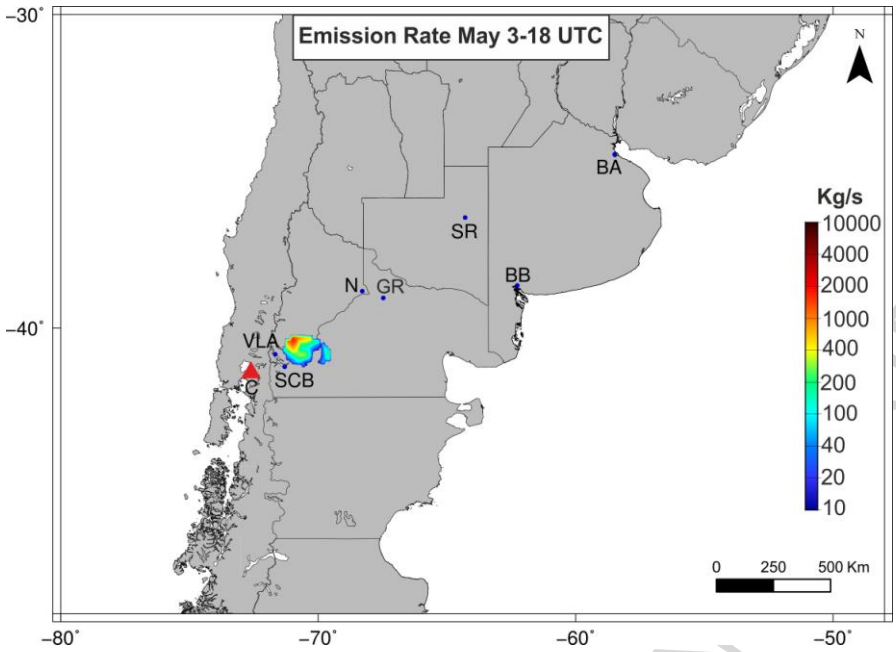

Fig. 12

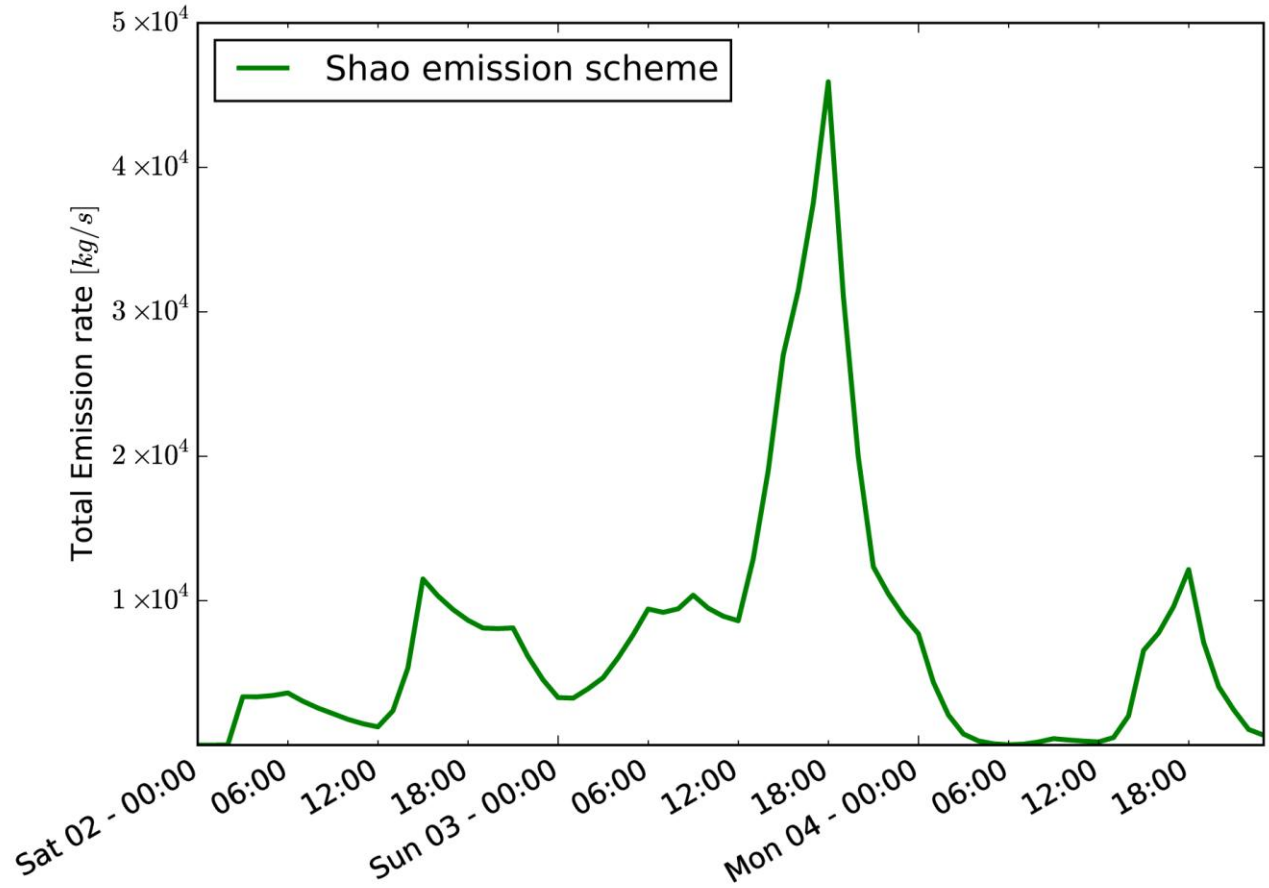

Fig. 13

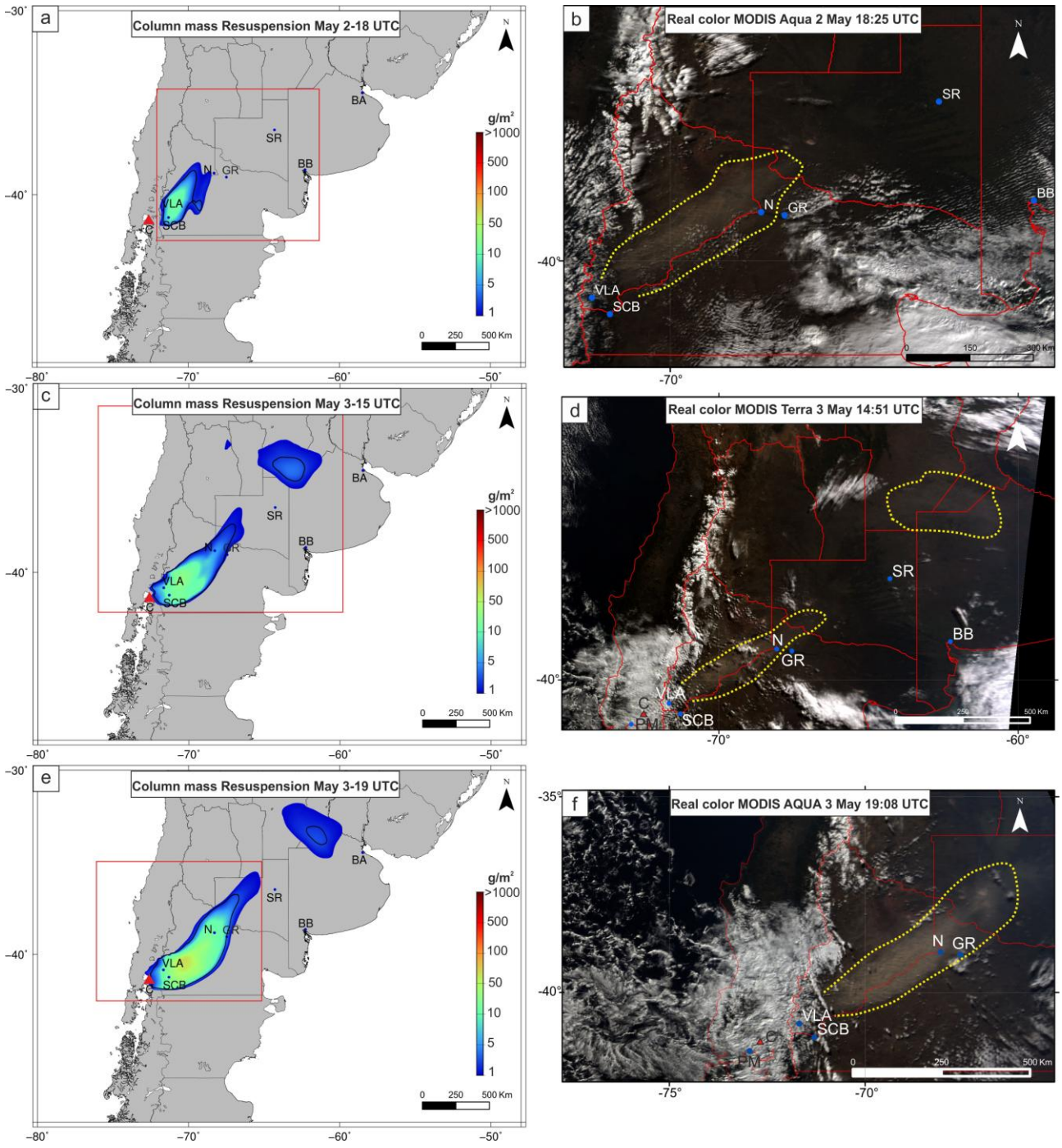

Fig. 14

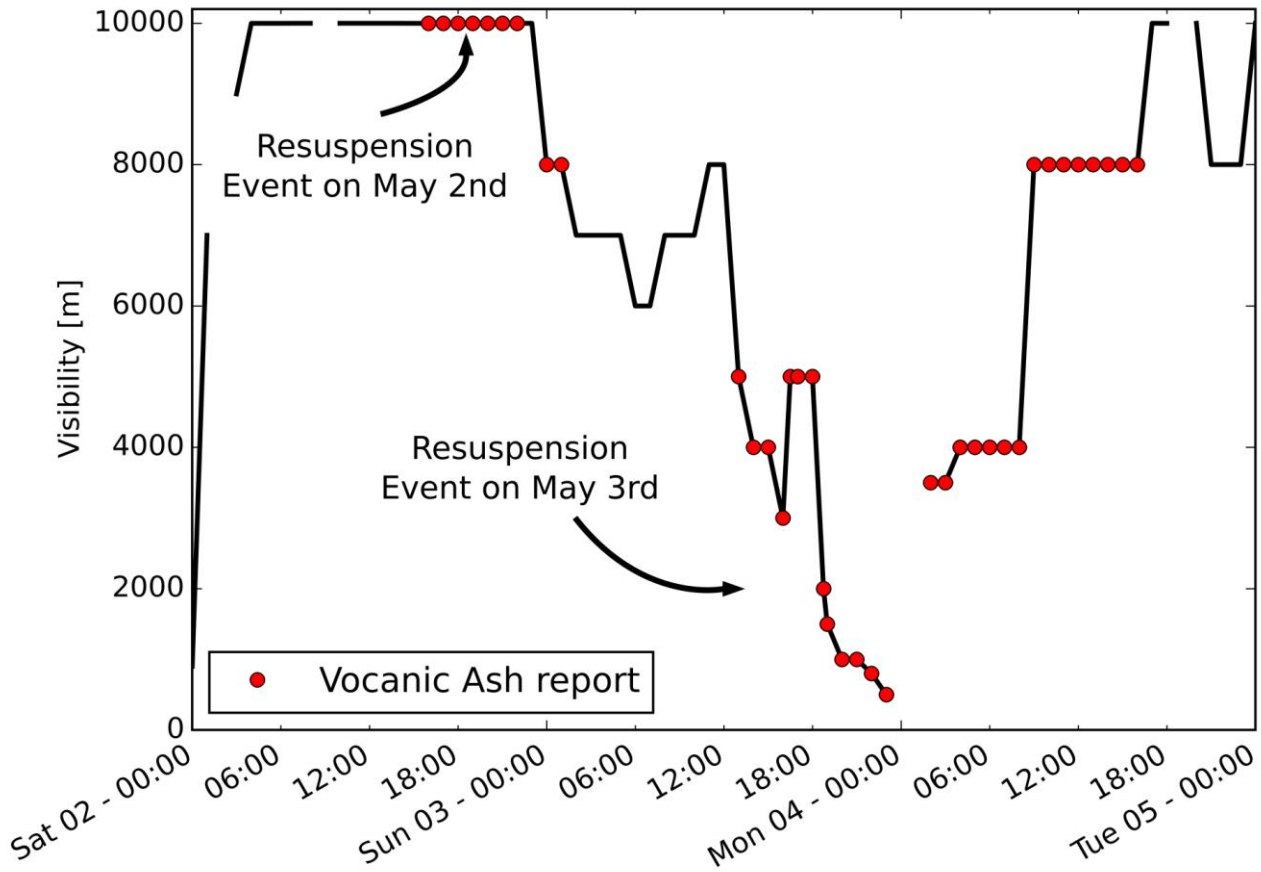

Fig. 15

Highlights:

- A numerical simulation was validated during the Calbuco eruption and resuspension.
- We reconstruct TGSD and consider aggregation process to improve results.
- Validation with satellite images and sample field data was performed.
- Results show the importance of having a complete database for different scenarios.